




Research Paper

Non-contact optical stiffness measurements in the organ of Corti in mice

Nina Chimienti^a, Chenjun Shi^b, Lily Kassis^c, Razzane Zaghoul^d, Man Do^e, Jitao Zhang^b,
 Xiying Guan^{c,e,*} 

^a Department of Biological Sciences, Wayne State University, Detroit, MI, USA

^b Department of Biomedical Engineering, Michigan State University, East Lansing, MI, USA

^c Department of Communication Sciences and Disorders, Wayne State University, Detroit, MI, USA

^d School of Medicine, Wayne State University, Detroit, MI, USA

^e Department of Biomedical Engineering, Wayne State University, Detroit, MI, USA

ARTICLE INFO

Keywords:

Brillouin microscopy
 Organ of Corti
 Stiffness
 Mechanical property
 in situ

ABSTRACT

Cochlear macromechanics and micromechanics both rely on the mechanical properties of the cells and membranes in the organ of Corti (OC). These components' stiffness have been investigated primarily using contact-based tests, which require the organ or cells to be removed from the cochlea. The approach is not only challenging but may alter the cells' stiffness as they are moved into a non-native environment. Recently, optical Brillouin microscopy has emerged as a promising tool for quantifying the mechanical property of biological specimens. This contact-free modality encourages that the stiffness of the OC cells and other components can be measured in situ and even in vivo. In the present study, we validated the feasibility of in situ Brillouin measurement on the OC cells' stiffness using fixed mouse cochleae. The results demonstrate that Brillouin microscopy has sufficient penetration depth and mechanical sensitivity to probe the OC, allowing us to differentiate the stiffness between the bone, spiral ligament, and cells; the longitudinal modulus obtained from the experiment varies between different types of OC cells in a way expected from the cells' cytoskeletal composition. This pilot study paves the way for future application of Brillouin microscopy to quantify the stiffness of OC constituents in situ in living cochleae.

1. Introduction

The vibration of the basilar membrane and the transmission of the vibration from the basilar membrane to the stereocilia depend on the mechanical properties of individual cells and membranes in the organ of Corti (OC) (Brownell 1997; Patuzzi 1996). It is hence of great importance to learn about their mechanical properties. The previous methodologies aiming to gain such information generally fall into three categories: inference from cytoskeletal molecules, direct mechanical test, and deduction through modeling and vibration data. Cytoskeletal molecules, such as microtubules and actins, and their arrangements in hair cells, supporting cells, and membranes in the OC have been examined using immunohistology and electron microscopy (Engström and Wersäll 1958; Tilney et al., 1980; Hirokawa and Tilney 1982; Slepecky and Chamberlain 1982; 1985; Slepecky and Ulfendahl 1992; Furness and Hackney 1990; Furness et al. 1990; Troutt et al. 1994; von Lubitz 1981; Raphael and Altschuler 1991; Flock et al. 1982; 1986; Holley et al. 1992; Arnold and Anniko 1990). Those studies reveal

mechanical heterogeneity in the OC and provide insights into the mechanical properties of individual constituents in the organ. But to quantify the properties, observation alone is not enough. Direct mechanical tests thus have been performed on individual components or the intact organ. When an individual cell is tested, it is often isolated from the OC and anchored to a measurement platform (Holley and Ashmore 1988; Tolomeo et al. 1996; Tolomeo and Holley 1997). This method allows one to interrogate the cell's stiffness, however, the stiffness of an *ex situ* cell may differ from when it resides in its natural habitat because the cell-cell and cell-extracellular matrix (ECM) adhesions and the microenvironment significantly influence the cell's cytoskeleton (Giancotti and Ruoslahti 1999; Humphrey et al. 2014). On the other hand, when an intact OC is measured, a probe is often used to press the reticular laminar or basilar membrane. The diameter of the tip of the probe and the excursion of the probe are limited to a few microns (Babahosseini et al. 2022; Sugawara et al. 2004; Szarama et al. 2012) to ensure the stiffness sensed by the probe is contributed mainly by the in-contact, local substance such as the apex of a single hair cell. This

* Corresponding author.

E-mail address: xiying.guan@wayne.edu (X. Guan).

<https://doi.org/10.1016/j.heares.2025.109520>

Received 23 September 2025; Received in revised form 8 December 2025; Accepted 22 December 2025

Available online 23 December 2025

0378-5955/© 2025 Published by Elsevier B.V.

method thus assesses the surface stiffness of a cell or the basilar membrane but does not measure the mechanical property of the structures a few microns beneath the surface. Therefore, the stiffness of, for example, the soma of hair cells and supporting cells cannot be obtained with this method. Lastly, computational models of the OC have been created to simulate sound-induced vibrations in the structure. The requirement of matching the simulated results with the experimental measurements (Olson et al. 2025; Zhou et al. 2022; He et al. 2018) - especially the recent data acquired with optical coherence tomography - constrains and thus could help infer the mechanical properties of the OC components (Zhou et al. 2022; Samaras et al. 2023; Bowling et al. 2021). However, because the dynamics in the OC is a multivariable problem, one set of mechanical properties yielding good simulations may not be the unique solution. In fact, the parameters used by different laboratories can vary drastically. For instance, in two state-of-the-art models the Young's modulus of the outer hair cell soma differ by ~2000 times (5000 Pa in Zhou et al. 2022 vs 2.7 Pa in Bowling et al. 2021) for the cell located 1 cm away from the stapes in gerbil cochlea. In short, the mechanical properties of individual OC components have not been fully characterized, and there is no consensus on them. The lack of knowledge hinders our understanding of the dynamics in the organ and the mechanism underlying the cochlear traveling wave.

Recently, confocal Brillouin microscopy has emerged as a contact-free and label-free method for characterizing the mechanical properties of live biological tissues (Kabakova et al. 2024; Prevedel et al. 2019; Zhang and Scarcelli 2021; Shi et al. 2023). It uses a laser beam to probe the sample's mechanical properties at the cellular and subcellular levels. Its working principle is based on the process of spontaneous Brillouin scattering, where the incident light interacts with the inherent acoustic waves inside the sample (due to spontaneous thermal fluctuations) and results in a frequency shift (i.e., Brillouin shift) to the outgoing scattered light (Dil 1982). As the propagation of the acoustic wave depends on the material's mechanical properties, the Brillouin shift is directly related to the longitudinal modulus and thus sheds light on the material's tensile stiffness (Zhang and Scarcelli 2021). Because of the all-optical, non-contact measurement modality, Brillouin microscopy has the potential to measure the mechanical properties of a cell and its surrounding structures without separating them from the natural milieu.

The present study aims to demonstrate a proof-of-concept measurement on the axial stiffness of OC components in the cochlea using confocal Brillouin microscopy. To support accurate anatomical targeting, we incorporated fluorescent labeling, and performed the measurement on fixed, decalcified cochlea specimens. We extracted fresh murine cochleae, fixed and decalcified them, cut each specimen into two halves, and added fluorescent markers to label hair cells and supporting cells. Then we use Brillouin microscopy to measure the longitudinal modulus of individual components in the OC in situ. The results show that the stiffness varies across different cell types and membranes. This study paves the way for future Brillouin assessment on the OC when it is in physiological condition.

2. Methods

2.1. Preparation of cochlea

The experimental protocol was approved by the Institutional Animal Care and Use Committee of Wayne State University. Sixteen C57BL/6 mice from eight to twelve weeks were used in this study. Thirteen of them were used to develop the technique for cochlea dissection, establish the method for fixation and immunostaining, and test and refine the protocol for Brillouin imaging. Three cochleae from the rest of the animals - labelled as M20R, M26R, and M32R - were investigated successfully using the matured Brillouin imaging protocol. To prepare the cochlea, the animals were euthanized using isoflurane gas followed by cervical dislocation. Upon euthanasia, the inner ear was harvested and fixed immediately in 4 % PFA at 4 °C for 24 h. Then the specimen was

rinsed three times with 1x PBS for 10 min each and decalcified in 120 mM EDTA (pH 7.2.–7.4) for 48–72 h (Yu et al. 2021). After decalcification, the specimen was rinsed in 1x PBS, and the vestibule and excess bone surrounding the cochlea were removed. The cochlea was separated into apical and basal halves using a 5 mm Vannas spring scissors and a scalpel (Montgomery and Cox 2016).

2.2. Immunostaining

Immunostaining was performed on some specimens to better recognize hair cells and supporting cells and thus helping establish coordinates for Brillouin scans. To prepare for immunostaining, the semi-cochlea was incubated at room temperature for one hour in blocking solution (made of 1x PBS, 0.1 % Triton X-100 and 5 % DK serum). The specimen was then incubated for 14–16 h at 37 °C with primary antibody cocktail of rabbit polyclonal antibody Myosin 7a (for inner and outer hair cells) and rat Sox2 (for supporting cells), followed by a secondary antibody cocktail containing Cy3 (conjugated to Myosin 7a) and AlexaFluor 488 (conjugated to Sox2) (Lieberman and Lieberman 2015).

2.3. Brillouin imaging

Both fluorescent and Brillouin imaging were performed using an Olympus IX83 confocal microscope equipped with fluorescent capacity and an add-on Brillouin module. The instrumentation of the Brillouin channel was detailed in the previous work (Zhang and Scarcelli, 2021). Fig. 1 illustrates the specimen setup and the simplified schematic for Brillouin imaging. Briefly, a 660-nm, 30-mW laser, as the incident light, passed through the objective lens and focused on a small volume (on the order of ~one μm^3) within the specimen. The specimen's inherent acoustic wave in that volume produced a frequency shift Ω_B (i.e., Brillouin shift) to the outgoing scattered light (Dil 1982). The light scattered back to the lens was guided to a homemade Brillouin spectrometer (Fig. 1) to extract Ω_B . The sample stage (H117, Prior Scientific) of the microscope was motorized (with resolution of 0.01 μm), allowing us to obtain, in theory, a three-dimensional (3D) map of the Brillouin shift of the specimen with a spatial resolution of one μm (limited by the optical resolution). However, because the dwell time per probing volume in the current setup is 40–100 ms (Zhang and Scarcelli, 2021), acquiring the 3D map of a $100 \times 100 \times 20 \mu\text{m}^3$ volume, for example, would take 2–5 h. We therefore obtained a few two-dimensional (2D) Brillouin scans per region of interest in the OC.

2.4. Protocol for imaging

Only the apical halves of the cochleae were used for imaging. The specimen was submerged in PBS in a 20 mm glass dish with the basilar membrane facing towards the microscope's objective lens (Fig. 1), and fluorescent signals, when available, were imaged first. Regions where the cells appeared normal with distinguishable boundaries were selected for Brillouin imaging. Once a targeted region was determined, a coarse Brillouin 2D scan ($5 \times 5 \mu\text{m}^2$ per pixel) perpendicular to the basilar membrane, along the cochlea's radial direction - represented by the yellow line in the inlet in Fig. 1- was performed in the region to assess the integrity of the cochlear partition. Such scans are referred to as YZ or radial scans in the rest of the report. Then a fine 2D scan ($1 \times 1 \mu\text{m}^2$ per pixel) in the same plane was performed to acquire a higher-resolution image. After that, one or two fine scans along the cochlea's longitudinal direction in the same region were performed. Those scans intersected hair cells and/or supporting cells are referred to as XY or longitudinal scans in the remaining texts. Representative fluorescent and 2D Brillouin images can be found in the results section.

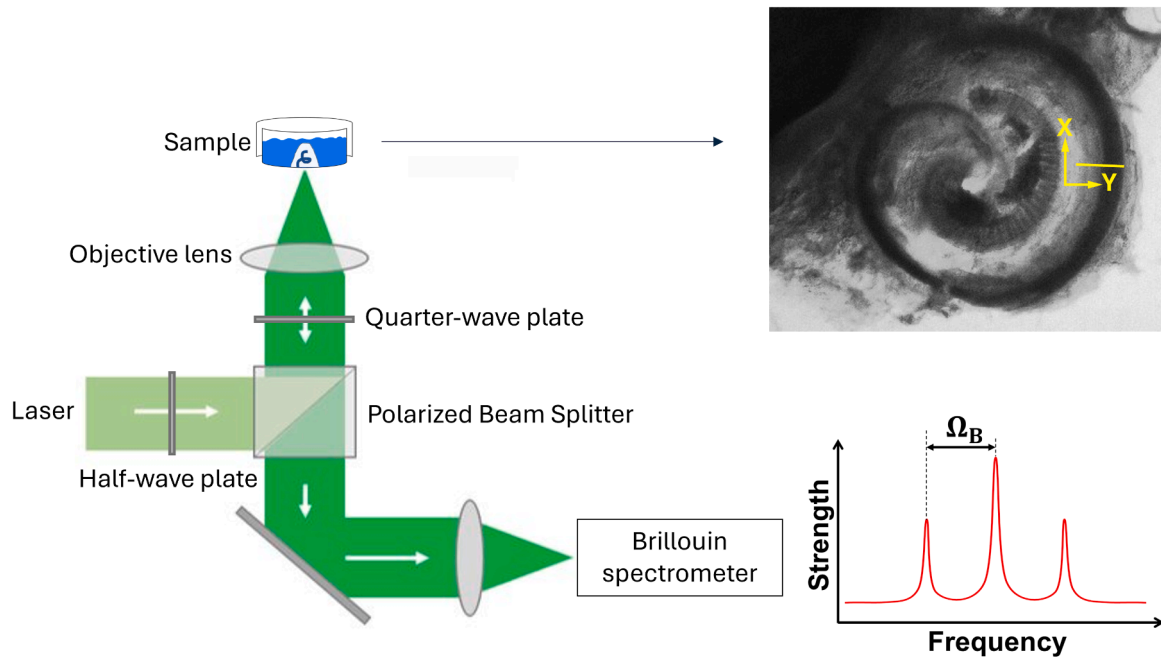


Fig. 1. Schematic of the experimental setup. The Brillouin incident light (laser) interacts with the sample’s inherent acoustic waves in the probing volume, producing a frequency shift Ω_B in the scattered light that is detected by the Brillouin spectrometer. The top-right inset is a representative brightfield image of a cochlea middle turn with the yellow line indicating the location of a radial scan.

2.5. Calculate mechanical modulus from Brillouin shift

MATLAB R2022a (The MathWorks, Natick, MA) was used to create 2D Brillouin images, and the color of each pixel represents the local Brillouin shift Ω_B (in Hz). Subsequently, Ω_B of the pixels of interests were used to compute the high-frequency (on the order of GHz) longitudinal modulus M and the quasi-static Young’s modulus E . In backward scattering geometry, Brillouin shift is determined by the sound velocity V in the material:

$$\Omega_B = \frac{2n}{\lambda} V,$$

where λ is the wavelength (in m) of the incident light in air, and n in the refractive index of the material. Furthermore, the sound velocity is associated with the longitudinal modulus M :

$$V = \sqrt{\frac{M}{\rho}},$$

where ρ is the density of the material (in kg/m^3). As a result, the longitudinal modulus can be derived by

$$M = \rho \lambda^2 \Omega_B^2 / (4n^2) \tag{1}$$

Both ρ and n depend on the materials in the probed volume, but among biological tissues the variation in the ratio ρ/n^2 is insignificant (Scarcelli et al. 2011; 2015; Webb et al. 2017; Conrad et al. 2019). Here ρ/n^2 was treated as a constant of $563 kg/m^3$ (Scarcelli et al. 2011).

The high-frequency longitudinal modulus M cannot be directly interpreted as the quasi-static Young’s modulus E , but strong correlation between the two has been observed in cells and tissues such as fibroblasts (Scarcelli et al. 2015), cornea (Webb et al. 2017), eye lens (Scarcelli et al. 2011), and tumor nodules (Conrad et al. 2019). When the sample’s condition changes (such as age or osmolality), those two moduli alter in the same direction. Fig. 2 illustrates the correlation between Brillouin-derived M and mechanically measured E in the previous studies (Scarcelli et al. 2011; 2015; Webb et al. 2017; Conrad et al. 2019).

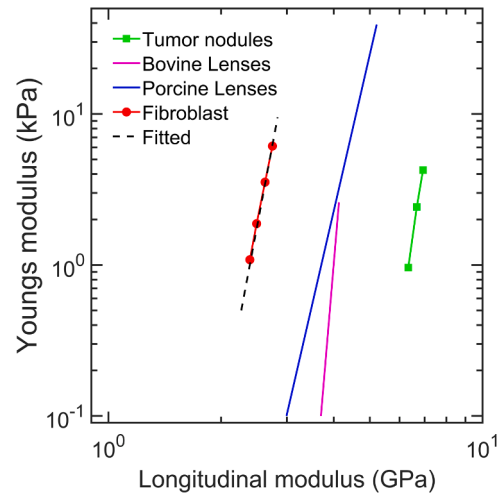


Fig. 2. Correlation between longitudinal modulus and Young’s modulus reported in previous studies for tumor nodules (Conrad et al. 2019), bovine and porcine lenses (Scarcelli et al. 2011), and fibroblasts (Scarcelli et al. 2015). The dashed line represents the fitted relationship between the two moduli in the fibroblasts.

The result suggests that, first, when changing the biological condition in a given type of sample, E changes linearly with M on a log-log plot, therefore, their relationship can be represented by a simple equation

$$\log_{10} E = a \log_{10} M + b \tag{2}$$

where a is the slope of an individual line in Fig. 2, and b the y-intercept. Second, while the slope a appears similar between different types of samples, b varies substantially. Therefore, a and, particularly, b need to be experimentally determined for a specific type of tissue when using M to estimate E .

Although a and b for the OC are unknown yet, we observed that M of

the OC cells and tissues varies in the range of 2–3 GPa (see results below), similar to that in the fibroblasts (dashed line in Fig. 2). Hence, we used the constants $a = 13.158$ and $b = -120.395$ fitted to the fibroblast data to estimate E (in Pa) from M' (in Pa) for the cochlea using

$$E = M^a \times 10^b \quad (3)$$

3. Results

3.1. Representative fluorescent and Brillouin images

Fig. 3 shows representative fluorescent and Brillouin images taken from one region in specimen M20R. Fig. 3A displays the fine radial Brillouin scan from that region, and the colors represent the Brillouin shift Ω_B . The image clearly shows that the Brillouin microscopy can penetrate the organ, and immediately, a few cochlear landmarks can be identified: on the far left is the spiral lamina, on the opposite the spiral ligament, and the cochlear partition is anchored in between. Importantly, this colormap of Ω_B represents the stiffness variation in the region: the bony spiral lamina is the stiffest (with highest Ω_B); the spiral ligament, mainly comprising fibrocytes and extracellular matrix, is softer; the cochlear partition, the mobile apparatus for mechano-transduction, is of the least overall stiffness. The difference in the mechanical property suggested by the Brillouin image concurs with that expected from the constituents or functions of those structures.

The two dashed lines in Fig. 3A mark where the two longitudinal Brillouin scans took place. Fig. 3B shows the Brillouin image of the top scan, accompanied by the hair-cell fluorescent image (Myosin 7a) of the same region shown in Fig. 3C. The side-by-side comparison confirms that the top Brillouin scan images the inner and outer hair cells and it also captures the pillar cells which are absent in the fluorescent image

(the gap between the inner and outer hair cells in Fig. 3C).

Fig. 3D shows the Brillouin image of the lower longitudinal scan, paired with the supporting cell fluorescent image (Sox2) shown in Fig. 3E. The correlation between the two asserts that the lower Brillouin scan captures the supporting cells on both sides of the tunnel including the inner pillar cells, the outer pillar cells, and the Deiters' cells. These longitudinal scans provide multiple samples of each cell type in the OC and thus allow us to better quantify the cells' stiffness than the radial scan.

3.2. Stiffness of the cells in the organ of Corti

Fig. 4A summarizes the longitudinal modulus M' of a variety of OC cells and the basilar membrane measured from Brillouin images on the middle turn of three cochleae. Each data point represents the mean value of M' across 8–10 cells of the same type sampled from longitudinal scans in a specimen, except that the basilar-membrane data are obtained from radial scans. The horizontal bar in each category represents the average M' over the three specimens, accompanied by \pm one standard deviation displayed as the vertical line. The Brillouin scans of the three specimens and the selection of cells and membrane for quantifying their M' are provided in supplementary Figs. 1–3, and the M' of individual cells in those specimens are displayed in supplementary Fig. 4.

The results show that the OC's longitudinal modulus in those scanned sites ranges from 2.4 to 2.54 GPa, with variations across different cell types: in general, the inner and outer pillar cells are of the highest modulus, while the outer hair cells are of the lowest. The Deiter's cells, the inner hair cells, and the basilar membrane's moduli are moderate and comparable.

Fig. 4B shows the Young's modulus E converted from the data in Fig. 4A using Eq. (3). The E in the OC ranges from 1 to 2.2 kPa, and it

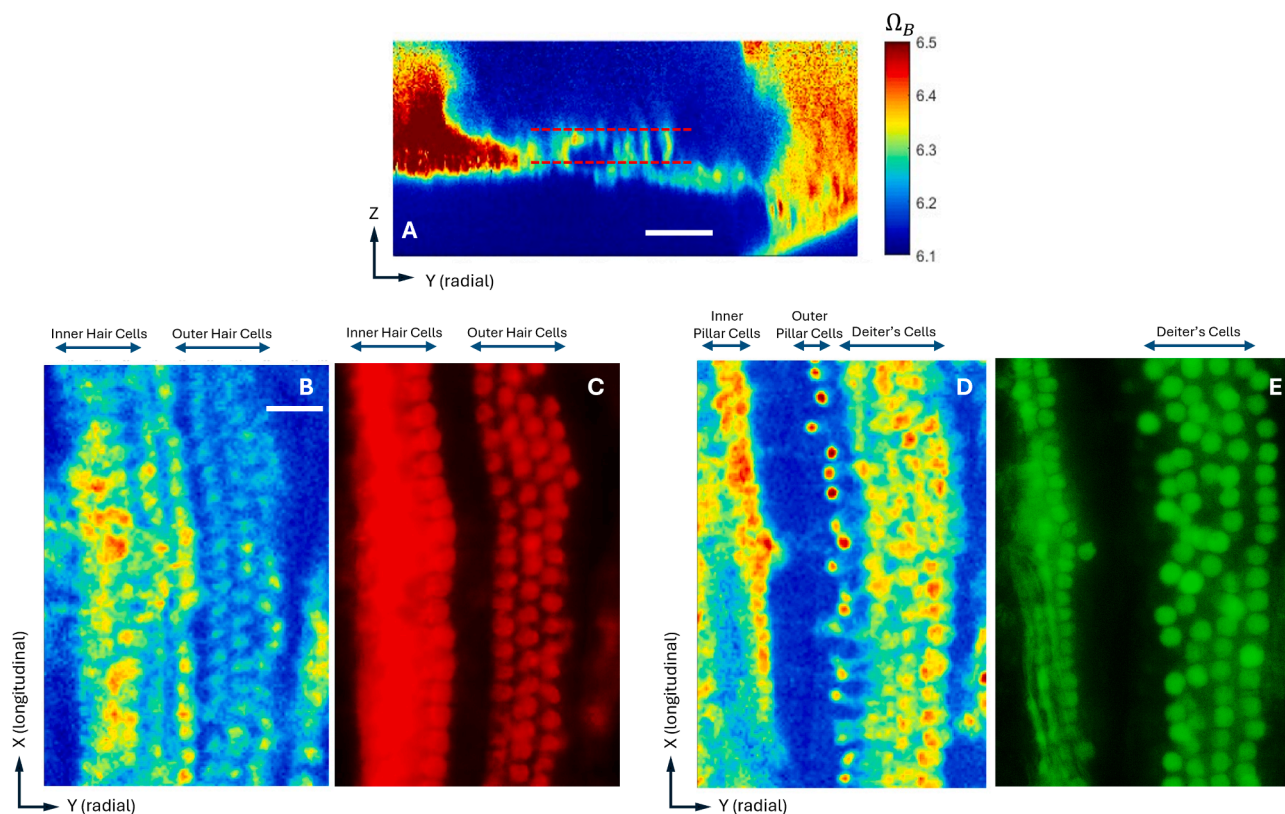


Fig. 3. Representative Brillouin and fluorescent images from a mouse cochlea (M20R). (A) A fine radial scan on the organ of Corti (OC); (B) a fine longitudinal scan mainly targeting hair cells and (C) myo7a-fluorescent image from the same region; (D) a fine longitudinal scan targeting supporting cells and (E) sox2-fluorescent image from the same region. The colors in the Brillouin images represent the Brillouin shift Ω_B ; the scale bar in (A) is 50 μm ; the scale bar in (B) is 20 μm and applicable in (C)-(E).

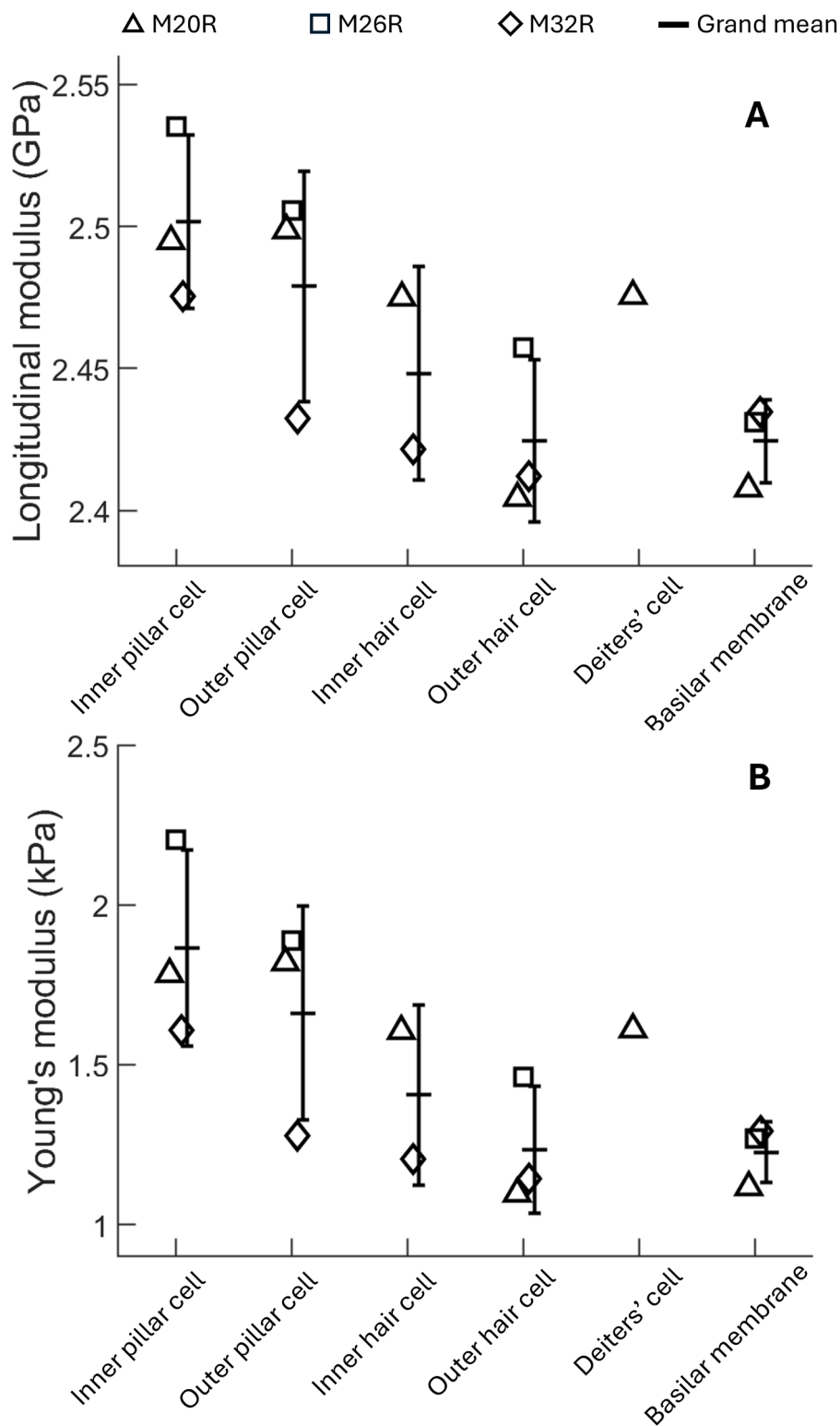


Fig. 4. (A) Mean and grand-mean longitudinal modulus of the basilar membrane and a variety of cells in the organ of Corti measured from the middle turns of three cochleae. (B) Mean and grand-mean Young's modulus converted from the longitudinal modulus using the correlation between the two moduli obtained in fibroblasts (Scarcelli et al. 2015).

varies over cell types in the same manner as the longitudinal modulus. Overall, the data in Fig. 4 suggest that the pillar cells are the OC's stiffest structure, followed by the Deiters' cells and the inner hair cells. The stiffness of the basilar membrane is in the same range as the inner hair cells. The outer hair cells appear to be the softest component in the organ.

A few limitations need to be noted here. First, the basilar membrane was the only structure quantified from radial scans, which were not as detailed as the longitudinal scans. Second, the Deiters' cells were only quantified in one sample (M20R, see supplementary Fig. 1); they were not measured in the other specimens because the OCs slanted and the longitudinal scans that were performed did not intersect the region of

the Deiters' cells (see supplementary Figs. 2 and 3). Third, prior to imaging, the specimens were fixed with PFA. Due to the chemical's crosslink effect, the Young's moduli in Fig. 4B may be higher than those in untreated fresh cochleae.

4. Discussion

The stiffness heterogeneity in the OC cells has been speculated previously by examining the two major cytoskeletal components -microfilaments and microtubules. In laboratory animals, these two structural filaments are most abundant in pillar and Deiters cells, and they are arranged longitudinally in the cell, run throughout the trunk of the cell, and are apparent in electron microscopic images (Lim 1986; Angelborg and Engström 1972; Engström and Wersäll 1953; 1958; Arima et al. 1986). The number of microfilaments and microtubules in Deiters cells, however, is smaller than that in pillars (Engström and Wersäll 1958), suggesting the pillar cells are the most rigid cells in the OC, followed by the Deiters. On the other hand, such end-to-end filaments in the inner and outer hair cells are much fewer and thus can be hardly seen under electron microscopy (Furness et al. 1990; Lim 1986; Engström and Wersäll 1953; 1958; Thorne et al. 1987; Steyger et al. 1989). They can be routinely observed in the sensory cells only by immunochemical labeling (Slepecky and Chamberlain 1982; Slepecky and Ulfendahl 1992; Flock et al. 1982; Steyger et al. 1989). The scarcity of microfilaments and microtubules in the bodies of inner and out hair cells indicate these cells' low-stiffness nature.

Due to the condition and the limited number of specimens used in the present work and the scarcity of relevant measurements in literature, the stiffness data in Fig. 4 are not ready for statistical analysis or comparison with other studies. There were only a few studies conducting mechanical tests on cochlear cells in guinea pigs: uniaxial compression tests on freshly isolated guinea-pig outer hair cells suggest that their Young's modulus, on average, is less than 500 Pa (Holley and Ashmore 1988), and the Young's modulus of fresh guinea-pig outer pillar cells deduced from bending tests is on the order of MPa (Tolomeo and Holley 1997). It is unclear if such drastic difference in the mechanical property can transfer to mouse cochleae, but the trend of variation in the longitudinal or Young's modulus among different types of OC cells observed in the present study, in general, aligns with the stiffness difference implied by the cytoskeletal evidence, suggesting the Brillouin microscopy has the potential to quantify the cells' mechanical property not only in fixed cochleae but also in fresh specimens.

What is perhaps more exciting and significant about this technology is that it is optical and contact-free, and therefore may enable live, in situ measurement and even in vivo measurement on individual OC cells in future studies. Being able to keep the organ in its original place brings a few crucial advantages. First, in conventional contact-based mechanical tests such as atomic force microscopy (Babahosseini et al. 2022), the OC or the OC cells need to be painstakingly separated from the cochlea, stabilized on a substrate or platform, and submerged in culture medium. Here we demonstrated that with Brillouin microscopy the organ can be measured in situ, which greatly simplifies the sample preparation and significantly reduces the risk of cell or structural damage. Second, since it is anchored between the spiral lamina and the spiral ligament, the OC is likely preloaded by a force which may stretch the cells and thus increase their stiffness. If the OC is in situ, this added stiffness due to the preload is preserved and can be captured by Brillouin imaging (it has been shown that the Brillouin shift is sensitive to shape change in cells (Scarcelli et al. 2015; Conrad et al. 2019)). If the OC is dissected out, the preload force may diminish or vanish, and the mechanical property could thus be underestimated. Third, we verified that the Brillouin light has an apt penetration ability, and this may allow one to measure the OC cells' stiffness through the round window membrane while the inner ear is kept intact. Although challenging, such measurement may be plausible in vivo or on excised inner ears. In either case the assessment would be limited to the cochlea base, but the physiological disturbance is much

smaller than that in an exposed OC, and the results are likely to be more faithful.

Besides the benefits, we recognized a few shortcomings and challenges in the experiments. First, the relationship between the high-frequency longitudinal modulus M' measured by Brillouin microscopy and the Young's modulus E is empirical and can differ from one tissue type to another (Scarcelli et al. 2011; 2015; Webb et al. 2017; Conrad et al. 2019). In the present study we converted M' to E for the cochlear cells using the two moduli's correlation measured in fibroblasts, which may suffice for a proof-of-concept study but will be inadequate if one wants to determine the bona fide Young's moduli using this technology. The relationship between M' and E for the cochlear constituents must be established experimentally before conducting a full-blown Brillouin assessment. Second, the Brillouin microscopy measures the sample's Brillouin shift and longitudinal modulus only in the direction of the incident light (the z direction in the present study). In our current setup, the angle between the cells' longitudinal axis and the light is small, and the measurement can thus be amended by the cosine of the angle. But if a target's stiffness mostly lies in a direction perpendicular to the light (such as the basilar membrane), the orientation of the specimen needs to be adjusted substantially to reduce the angle. Another notable challenge we encountered was the extended time required for the fine scans. For live-cell imaging, this constraint would force one to prioritize the targets for imaging and might risk the specimen's health. One way to mitigate it is to reduce the scan's resolution (larger space represented by each pixel), but a time-resolution balance needs to be found to ensure the scan captures enough structural details. Furthermore, the use of fluorescent tags proved to be helpful for identifying cell types and their respective appearances in Brillouin scans. This aid will not be available during in situ, live-tissue measurements in wildtype specimens, so gaining familiarity with the location of the organ of Corti from solely brightfield visuals is crucial for future experiments with living cochleae.

5. Conclusion

In the present study, we tested the feasibility of Brillouin microscopy for measuring the stiffness of a variety of OC cells. Mouse cochleae were fixed, decalcified, and dissected to fully expose the OC, and Brillouin scans were taken on the middle turn of the specimen. The results showed that the Brillouin microscopy can differentiate the stiffness between the bone, ligament, and sensory epithelium in the cochlea, and the longitudinal and Young's moduli derived from the Brillouin shift vary between different types of OC cells in a manner consistent with the cytoskeletal diversity among those cells. Therefore, we believe Brillouin microscopy can potentially be used to quantify the mechanical property of living cells and membranes in the cochlea in situ and in vivo. Knowing the property will help us better understand the underlying mechanism of the cochlear traveling wave and the transmission of vibration in the OC.

CRedit authorship contribution statement

Nina Chimienti: Writing – review & editing, Writing – original draft, Methodology, Formal analysis, Data curation. **Chenjun Shi:** Writing – review & editing, Software, Methodology, Formal analysis, Data curation. **Lily Kassis:** Writing – review & editing, Writing – original draft, Methodology, Formal analysis, Data curation. **Razzane Zaghoul:** Methodology. **Man Do:** Methodology, Data curation. **Jitao Zhang:** Writing – review & editing, Supervision, Methodology, Conceptualization. **Xiying Guan:** Writing – review & editing, Writing – original draft, Supervision, Methodology, Investigation, Formal analysis, Conceptualization.

Acknowledgement

This work is supported by Richard Barber Interdisciplinary Research Program (X.G. and J.Z.), National Institutes of Health R21HD112663 (J.

Z.), and National Science Foundation CBET- 2339278 (J.Z.).

Supplementary materials

Supplementary material associated with this article can be found, in the online version, at [doi:10.1016/j.heares.2025.109520](https://doi.org/10.1016/j.heares.2025.109520).

References

- Angelborg, C., Engström, H., 1972. Supporting Elements in the Organ of Corti I. Fibrillar Structures in the Supporting Cells of the Organ of Corti of Mammals. *Acta Otolaryngol.* 73 (sup301), 49–60. <https://doi.org/10.3109/00016487209122689>.
- Arima, T., Uemura, T., Yamamoto, T., 1986. Cytoskeletal Organization in the Supporting Cell of the Guinea Pig Organ of Corti. *Hear. Res.* 24 (2), 169–175. [https://doi.org/10.1016/0378-5955\(86\)90061-4](https://doi.org/10.1016/0378-5955(86)90061-4).
- Arnold, W., Matti, Anniko, 1990. Structurally Based New Functional Interpretations of the Subsurface Cisternal Network in Human Outer Hair Cells. *Acta Otolaryngol.* 109 (3–4), 213–220. <https://doi.org/10.3109/00016489009107436>.
- Babhosseini, H., Belyantseva, IA., Yousaf, R., et al., 2022. Unbalanced Bidirectional Radial Stiffness Gradients within the Organ of Corti Promoted by TRIOBP. *Proc. Natl. Acad. Sci.* 119 (26), e2115190119. <https://doi.org/10.1073/pnas.2115190119>.
- Bowling, T., Wen, H., Meenderink, SW.F., Dong, W., Meaud, J., 2021. Intracochlear Distortion Products Are Broadly Generated by Outer Hair Cells but Their Contributions to Otoacoustic Emissions Are Spatially Restricted. *Sci. Rep.* 11 (1), 13651. <https://doi.org/10.1038/s41598-021-93099-7>.
- Brownell, WE., 1997. How the Ear Works - Nature's Solutions for Listening. *Volta Rev.* 99 (5), 9–28.
- Conrad, C., Gray, KM., Stroka, KM., Rizvi, I., Scarcelli, G., 2019. Mechanical Characterization of 3D Ovarian Cancer Nodules Using Brillouin Confocal Microscopy. *Cell Mol. Bioeng.* 12 (3), 215–226. <https://doi.org/10.1007/s12195-019-00570-7>.
- Dil, J.G., 1982. Brillouin Scattering in Condensed Matter. *Rep. Prog. Phys.* 45 (3), 285. <https://doi.org/10.1088/0034-4885/45/3/002>.
- Engström, H., Wersäll, J., 1953. Structure of the Organ of Corti: 2. Supporting Structures and Their Relations to Sensory Cells and Nerve Endings. *Acta Otolaryngol.* 43 (4–5), 323–334. <https://doi.org/10.3109/00016485309119854>.
- Engström, H., Wersäll, J., 1958. Structure and innervation of the inner ear sensory epithelia. *Int. Rev. Cytol.* 7, 535–585. [https://doi.org/10.1016/S0074-7696\(08\)62695-9](https://doi.org/10.1016/S0074-7696(08)62695-9).
- Flock, Å., Bretscher, A., Weber, K., 1982. Immunohistochemical Localization of Several Cytoskeletal Proteins in Inner Ear Sensory and Supporting Cells. *Hear. Res.* 7 (1), 75–89. [https://doi.org/10.1016/0378-5955\(82\)90082-X](https://doi.org/10.1016/0378-5955(82)90082-X).
- Flock, Å., Flock, B., Ulfendahl, M., 1986. Mechanisms of Movement in Outer Hair Cells and a Possible Structural Basis. *Arch Otorhinolaryngol.* 243 (2), 83–90. <https://doi.org/10.1007/BF00453755>.
- Furness, D.N., Hackney, C.M., 1990. Comparative Ultrastructure of Subsurface Cisternae in Inner and Outer Hair Cells of the Guinea Pig Cochlea. *Eur. Arch. Oto-Rhino-Laryngol.* 247 (1), 12–15. <https://doi.org/10.1007/BF00240941>.
- Furness, DN., Hackney, CM., Steyger, PS., 1990. Organization of Microtubules in Cochlear Hair Cells. *J. Electron Microsc. Tech.* 15 (3), 261–279. <https://doi.org/10.1002/jemt.1060150306>.
- Giancotti, FG., Ruoslahti, E., 1999. Integrin Signaling. *Science* 285 (5430), 1028–1033. <https://doi.org/10.1126/science.285.5430.1028>.
- He, W., Kemp, D., Ren, T., 2018. Timing of the reticular lamina and basilar membrane vibration in living gerbil cochlea. *eLife* 7, e37625. <https://doi.org/10.7554/eLife.37625> (September).
- Hirokawa, N., Tilney, L.G., 1982. Interactions between actin filaments and between actin filaments and membranes in quick-frozen and deeply etched hair cells of the chick ear. *J. Cell Biol.* 95 (1), 249–261. <https://doi.org/10.1083/jcb.95.1.249>.
- Holley, M.C., Ashmore, J.F., 1988. A cytoskeletal spring in cochlear outer hair cells. *Nature* 335 (6191), 635–637. <https://doi.org/10.1038/335635a0>.
- Holley, M.C., Kalinec, F., Kachar, B., 1992. Structure of the cortical cytoskeleton in mammalian outer hair cells. *J. Cell Sci.* 102 (3), 569–580. <https://doi.org/10.1242/jcs.102.3.569>.
- Humphrey, JD., Dufresne, ER., Schwartz, MA., 2014. Mechanotransduction and extracellular matrix homeostasis. *Nat. Rev. Mol. Cell Biol.* 15 (12), 802–812. <https://doi.org/10.1038/nrm3896>.
- Kabakova, I., Zhang, J., Xiang, Y., Caponi, S., Bilencia, A., Guck, J., Scarcelli, G., 2024. Brillouin microscopy. *Nat. Rev. Methods Primers* 4 (1), 1–20. <https://doi.org/10.1038/s43586-023-00286-z>.
- Liberman, LD., Charles Liberman, M., 2015. Dynamics of cochlear synaptopathy after acoustic overexposure. *JARO: J. Assoc. Res. Otolaryngol.* 16 (2), 205–219. <https://doi.org/10.1007/s10162-015-0510-3>.
- Lim, DJ., 1986. Functional structure of the organ of Corti: a review. *Hear. Res.* 22 (1), 117–146. [https://doi.org/10.1016/0378-5955\(86\)90089-4](https://doi.org/10.1016/0378-5955(86)90089-4).
- Lubitz, DK.J., Ekström, 1981. Subsurface tubular system in the outer sensory cells of the rat cochlea. *Cell Tissue Res.* 220 (4), 787–795. <https://doi.org/10.1007/BF00210462>.
- Montgomery, SC., Cox, BC., 2016. Whole mount dissection and immunofluorescence of the adult mouse cochlea. *J. Vis. Exp.: JoVE* 107, 53561. <https://doi.org/10.3791/53561> (January).
- Olson, ES., Dong, W., Applegate, BE., et al., 2025. Visualizing motions within the cochlea's organ of Corti and illuminating cochlear mechanics with optical coherence tomography. *Hear. Res.* 455, 109154. <https://doi.org/10.1016/j.heares.2024.109154> (January).
- Patuzzi, R., 1996. Cochlear micromechanics and macromechanics. In: Dallos, P., Popper, A.N., Fay, R.R. (Eds.), *The Cochlea*. Springer, New York, pp. 186–257. https://doi.org/10.1007/978-1-4612-0757-3_4.
- Prevedel, R., Diz-Muñoz, A., Ruocco, G., Antonacci, G., 2019. Brillouin microscopy: an emerging tool for mechanobiology. *Nat. Methods* 16, 969–977. <https://doi.org/10.1038/s41592-019-0543-3>.
- Raphael, Y., Altschuler, RA., 1991. Reorganization of cytoskeletal and junctional proteins during cochlear hair cell degeneration. *Cell Motil.* 18 (3), 215–227. <https://doi.org/10.1002/cm.970180307>.
- Samaras, G., Wen, H., Meaud, J., 2023. Broad nonlinearity in reticular lamina vibrations requires compliant organ of corti structures. *Biophys. J.* 122 (5), 880–891. <https://doi.org/10.1016/j.bpj.2023.01.029>.
- Scarcelli, G., Kim, P., Yun, S.H., 2011. In vivo measurement of age-related stiffening in the crystalline lens by Brillouin optical microscopy. *Biophys. J.* 101 (6), 1539–1545. <https://doi.org/10.1016/j.bpj.2011.08.008>.
- Scarcelli, G., Polacheck, WJ., Nia, HT., et al., 2015. Noncontact three-dimensional mapping of intracellular hydromechanical properties by Brillouin microscopy. *Nat. Methods* 12 (12), 1132–1134. <https://doi.org/10.1038/nmeth.3616>.
- Shi, C., Zhang, H., Zhang, J., 2023. Non-contact and label-free biomechanical imaging: stimulated Brillouin microscopy and beyond. *Front Phys* 11, 1175653. <https://doi.org/10.3389/fphy.2023.1175653>.
- Slepecky, N., Chamberlain, SC., 1982. Distribution and polarity of actin in the sensory hair cells of the chinchilla cochlea. *Cell Tissue Res.* 224 (1), 15–24. <https://doi.org/10.1007/BF00217262>.
- Slepecky, N., Chamberlain, SC., 1985. Immunoelectron microscopic and immunofluorescent localization of cytoskeletal and muscle-like contractile proteins in inner ear sensory hair cells. *Hear. Res.* 20 (3), 245–260. [https://doi.org/10.1016/0378-5955\(85\)90029-2](https://doi.org/10.1016/0378-5955(85)90029-2).
- Slepecky, NB., Ulfendahl, M., 1992. Actin-binding and microtubule-associated proteins in the organ of Corti. *Hear. Res.* 57 (2), 201–215. [https://doi.org/10.1016/0378-5955\(92\)90152-D](https://doi.org/10.1016/0378-5955(92)90152-D).
- Steyger, P.S., Furness, D.N., Hackney, C.M., Richardson, G.P., 1989. Tubulin and microtubules in cochlear hair cells: comparative immunocytochemistry and Ultrastructure. *Hear. Res.* 42 (1), 1–16. [https://doi.org/10.1016/0378-5955\(89\)90113-5](https://doi.org/10.1016/0378-5955(89)90113-5).
- Sugawara, M., Ishida, Y., Wada, H., 2004. Mechanical properties of sensory and supporting cells in the organ of Corti of the guinea pig cochlea - study by atomic force microscopy. *Hear. Res.* 192 (1), 57–64. <https://doi.org/10.1016/j.heares.2004.01.014>.
- Szarama, KB., Stepanyan, R., Petralia, RS., et al., 2012. Fibroblast growth factor receptor 3 regulates microtubule formation and cell surface mechanical properties in the developing organ of Corti. *BioArchitecture* 2 (6), 214–219. <https://doi.org/10.4161/bioa.22332>.
- Thorne, PR., Carlisle, L., Zajic, G., Schacht, J., Altschuler, RA., 1987. Differences in the distribution of f-actin in outer hair cells along the organ of Corti. *Hear. Res.* 30 (2), 253–265. [https://doi.org/10.1016/0378-5955\(87\)90141-9](https://doi.org/10.1016/0378-5955(87)90141-9).
- Tilney, L.G., Derosier, D.J., Mulroy, M.J., 1980. The organization of actin filaments in the stereocilia of cochlear hair cells. *J. Cell Biol.* 86 (1), 244–259. <https://doi.org/10.1083/jcb.86.1.244>.
- Tolomeo, J.A., Holley, M.C., 1997. Mechanics of microtubule bundles in pillar cells from the inner ear. *Biophys. J.* 73 (4), 2241–2247. [https://doi.org/10.1016/S0006-3495\(97\)78255-9](https://doi.org/10.1016/S0006-3495(97)78255-9).
- Tolomeo, J.A., Steele, C.R., Holley, M.C., 1996. Mechanical properties of the lateral cortex of mammalian auditory outer hair cells. *Biophys. J.* 71 (1), 421–429. [https://doi.org/10.1016/S0006-3495\(96\)79244-5](https://doi.org/10.1016/S0006-3495(96)79244-5).
- Trout, L.L., Heumen, W.R.A., Pickles, J.O., 1994. The changing microtubule arrangements in developing hair cells of the chick cochlea. *Hear. Res.* 81 (1), 100–108. [https://doi.org/10.1016/0378-5955\(94\)90157-0](https://doi.org/10.1016/0378-5955(94)90157-0).
- Webb, JN., Su, JP., Scarcelli, G., 2017. Mechanical outcome of accelerated corneal crosslinking evaluated by Brillouin microscopy. *J. Cataract Refract. Surg.* 43 (11), 1458. <https://doi.org/10.1016/j.jcrs.2017.07.037>.
- Yu, HV., Tao, L., Llamas, J., et al., 2021. POU4F3 Pioneer Activity Enables ATOH1 to drive diverse mechanoreceptor differentiation through a feed-forward epigenetic mechanism. *Proc. Natl. Acad. Sci.* 118 (29), e2105137118. <https://doi.org/10.1073/pnas.2105137118>.
- Zhang, J., Scarcelli, G., 2021. Mapping mechanical properties of biological materials via an add-on Brillouin module to confocal microscopes. *Nat. Protoc.* 16, 1251–1275. <https://doi.org/10.1038/s41596-020-00457-2>.
- Zhou, W., Jabeen, T., Sabha, S., Becker, J., Nam, J.-H., 2022. Deiters cells act as mechanical equalizers for outer hair cells." research articles. *J. Neurosci.* 42 (44), 8361–8372. <https://doi.org/10.1523/JNEUROSCI.2417-21.2022>.